2018

Excellent structural, optical, and electrical properties of Nd-doped BaSnO3 transparent thin films

Fang-Yuan Fan
Shanghai Normal University

Weiyao Zhao
University of Wollongong, wz929@uowmail.edu.au

Ting-Wei Chen
Nanchang University

Jian-Min Yan
Chinese Academy Of Sciences

Jin-Peng Ma
Shanghai Normal University

See next page for additional authors

Publication Details

Fan, F., Zhao, W., Chen, T., Yan, J., Ma, J., Guo, L., Gao, G., Wang, F. & Zheng, R. (2018). Excellent structural, optical, and electrical properties of Nd-doped BaSnO3 transparent thin films. Applied Physics Letters, 113 (20), 202102-1-202102-5.

Excellent structural, optical, and electrical properties of Nd-doped BaSnO3 transparent thin films

Abstract
We epitaxially grew 7 mol. % Nd-doped BaSnO3 (NBSO) thin films on double-side polished SrTiO3 (001) single-crystal substrates and optimized the oxygen pressure (PO2), substrate temperature (TS), and film thickness (t) to achieve excellent structural, optical, and electrical performance. By keeping TS (=800 °C) constant, NBSO films prepared at PO2 = 10 Pa show the best crystallization, yielding a full-width at half-maximum (FWHM) of the x-ray diffraction rocking curve of 0.079° and exhibiting a room-temperature resistivity (ρ) of ~1.85 mΩ cm and a volume carrier density (n) of ~8.5 x 1020/cm3. By keeping PO2 (=10 Pa) constant, the room-temperature ρ of NBSO films could be reduced to as low as 0.5 mΩ cm by increasing TS from 700 to 825°; meanwhile, the volume carrier density and mobility show the maximum of 5.04 x 1020/cm3 and 24.9 cm2/Vs, respectively, for TS = 825 °C. For all as-grown NBSO thin films, the optical transmittance in the visible wavelength region is larger than 80%. The optimized comprehensive properties of the NBSO films with FWHM = 0.11°, ρ = 0.5 mΩ cm, μ = 24.9 cm2/Vs, and T > 80% are superior to those of other rare-earth and 4d- and 5d-transition metal-doped BaSnO3 thin films.

Disciplines
Engineering | Physical Sciences and Mathematics

Publication Details
Fan, F., Zhao, W., Chen, T., Yan, J., Ma, J., Guo, L., Gao, G., Wang, F. & Zheng, R. (2018). Excellent structural, optical, and electrical properties of Nd-doped BaSnO3 transparent thin films. Applied Physics Letters, 113 (20), 202102-1-202102-5.

Authors
Fang-Yuan Fan, Weiyao Zhao, Ting-Wei Chen, Jian-Min Yan, Jin-Peng Ma, Lei Guo, Guan-Yin Gao, Feifei Wang, and Ren-Kui Zheng

Excellent structural, optical, and electrical properties of Nd-doped $BaSnO_3$ transparent thin films

Fang-Yuan Fan, Wei-Yao Zhao, Ting-Wei Chen, Jian-Min Yan, Jin-Peng Ma, Lei Guo, Guan-Yin Gao, Fei-Fei Wang, and Ren-Kui Zheng

Citation: Appl. Phys. Lett. **113**, 202102 (2018); doi: 10.1063/1.5063538
View online: https://doi.org/10.1063/1.5063538
View Table of Contents: http://aip.scitation.org/toc/apl/113/20
Published by the American Institute of Physics

Excellent structural, optical, and electrical properties of Nd-doped $BaSnO_3$ transparent thin films

Fang-Yuan Fan,[1,2,a)] Wei-Yao Zhao,[3,a)] Ting-Wei Chen,[4] Jian-Min Yan,[2] Jin-Peng Ma,[1] Lei Guo,[2] Guan-Yin Gao,[5] Fei-Fei Wang,[1,b)] and Ren-Kui Zheng[4,c)]

[1]*Key Laboratory of Optoelectronic Material and Device, Department of Physics, Shanghai Normal University, Shanghai 200234, China*
[2]*State Key Laboratory of High Performance Ceramics and Superfine Microstructure, Shanghai Institute of Ceramics, Chinese Academy of Sciences, Shanghai 200050, China*
[3]*ISEM, Innovation Campus, University of Wollongong, Wollongong, NSW 2500, Australia*
[4]*School of Materials Science and Engineering, Nanchang University, Nanchang 330031, China*
[5]*Hefei National Laboratory for Physical Sciences at Microscale, University of Science and Technology of China, Hefei 230026, China*

(Received 28 September 2018; accepted 28 October 2018; published online 14 November 2018)

We epitaxially grew 7 mol. % Nd-doped $BaSnO_3$ (NBSO) thin films on double-side polished $SrTiO_3$ (001) single-crystal substrates and optimized the oxygen pressure (P_{O2}), substrate temperature (T_S), and film thickness (t) to achieve excellent structural, optical, and electrical performance. By keeping T_S (=800 °C) constant, NBSO films prepared at $P_{O2} = 10$ Pa show the best crystallization, yielding a full-width at half-maximum (FWHM) of the x-ray diffraction rocking curve of 0.079° and exhibiting a room-temperature resistivity (ρ) of ~1.85 mΩ cm and a volume carrier density (n) of $\sim 8.5 \times 10^{20}/cm^3$. By keeping P_{O2} (=10 Pa) constant, the room-temperature ρ of NBSO films could be reduced to as low as 0.5 mΩ cm by increasing T_S from 700 to 825°; meanwhile, the volume carrier density and mobility show the maximum of $5.04 \times 10^{20}/cm^3$ and 24.9 cm^2/Vs, respectively, for $T_S = 825$ °C. For all as-grown NBSO thin films, the optical transmittance in the visible wavelength region is larger than 80%. The optimized comprehensive properties of the NBSO films with FWHM = 0.11°, $\rho = 0.5$ mΩ cm, $\mu = 24.9\ cm^2/Vs$, and $T > 80\%$ are superior to those of other rare-earth and 4*d*- and 5*d*-transition metal-doped $BaSnO_3$ thin films. *Published by AIP Publishing.* https://doi.org/10.1063/1.5063538

The growing demand of optoelectronic devices such as flat-panel displays, light-emitting diodes, energy-efficient windows, and solar cells calls for high-performance and low-cost transparent conductive materials.[1–5] Currently, one of the popular approaches to combine high electrical conductivity with high optical transparency in the visible spectrum is the introduction of post-transition metal cations, e.g., Zn^{2+}, Cd^{2+}, In^{3+}, and Sn^{4+}(Refs. 6–8) into wide bandgap oxide semiconductors with small effective electron mass. It is well known that the Sn-doped In_2O_3 (ITO) has been widely used in optoelectronic devices because of its high transparency (>90%) in the visible spectrum and excellent electrical properties (conductivity $\sigma = 1 \times 10^4$ S cm^{-1}, electron concentration $n = 3 \times 10^{21}/cm^3$, and mobility $\mu = 20$–$100\ cm^2\ V^{-1}\ s^{-1}$).[7,9,10] However, ITO drawbacks such as high cost and relative chemical instability in the thermal reduction atmosphere are to be resolved.[11] Therefore, developing cheap and stable transparent conductive thin films with outstanding optical transparency and electrical conductivity and/or special structural properties is an on-going challenge.

In the past several years, perovskite-type compounds, e.g., titanates ($SrTiO_3$), vanadates ($Sr/CaVO_3$), and stannates ($Ca/Sr/BaSnO_3$),[12–17] become increasingly popular for their compatibility with perovskite-based optoelectronic devices. Among those compounds, $BaSnO_3$-based oxides have attracted growing attention due to their excellent properties: (1) $BaSnO_3$ possesses a wide bandgap of 3.4 eV and can be easily doped with electron carriers; (2) $BaSnO_3$ films can be epitaxially grown on a variety of lattice-mismatched perovskite substrates;[18–23] and (3) the conduction band of $BaSnO_3$ is mainly contributed by the Sn 5s orbital which has small effective electron mass, resulting in high electrical conductivity.[18] Upon cations' doping, the optical and electrical properties of $BaSnO_3$ films could be significantly improved. For instance, Liu *et al.*[19] substituted Sn with 7 mol. % Sb to decrease the room-temperature resistivity (ρ) from 8.0 to 2.4 mΩ cm, with an electron mobility of 1.75 $cm^2\ V^{-1}\ s^{-1}$. Similarly, replacing Sn with 6 mol. % Ta or 5 mol. % Nb yields room-temperature ρ = 2.25 and 0.48 mΩ cm for $BaSn_{0.94}Ta_{0.06}$[20] and $BaSn_{0.95}Nb_{0.05}O_3$[21] films, respectively.

On the other hand, replacing the Ba^{2+} ions with trivalent rare-earth ions also benefits the electrical conductivity of transparent $R_xBa_{1-x}SnO_3$ (R = rare-earth ions) films. For example, with the optimization of preparation parameters, the room-temperature mobility of 1 mol. % La-doped $BaSnO_3$ films grown on $BaSnO_3$ single-crystal substrates reaches 100 $cm^2\ V^{-1}\ s^{-1}$ with $n = 1.3 \times 10^{20}/cm^3$.[22] It is noted that the room-temperature μ of La-doped $BaSnO_3$ single crystals reaches 320 $cm^2\ V^{-1}\ s^{-1}$ with $n = 8 \times 10^{19}/cm^3$,[23] which means that there is possibility that the mobility of La-doped $BaSnO_3$ films could be further increased to a higher value.

[a)]Fang-Yuan Fan and Wei-Yao Zhao contributed equally to this work.
[b)]Electronic mail: ffwang@shnu.edu.cn
[c)]Electronic mail: zrk@ncu.edu.cn

Besides, other trivalent rare-earth ions' doping has been carried out for $BaSnO_3$ thin films, e.g., Li *et al.* reported that 4 mol. % Sm-doped $BaSnO_3$ films grown on MgO substrates have an optical transmittance of 80% and a room-temperature ρ of ~7.8 mΩ cm.[24] Liu *et al.* found that $Ba_{0.93}Gd_{0.07}SnO_3$ films grown on MgO substrates have an optical transmittance of 80% and a room-temperature ρ of ~6.2 mΩ cm.[25] Although previous studies have demonstrated that La, Sm, and Gd doping could improve the conductivity of $BaSnO_3$ films, it is still unknown whether other rare-earth ion doping could further improve the electrical and optical properties of $BaSnO_3$ films or not. Particularly, the effects of Nd^{3+} ion doping on the electrical and optical transmittance properties of $BaSnO_3$ films are still missing.

In this work, we systematically optimized the growth parameters for 7 mol. % Nd-doped $BaSnO_3$ thin films with different thicknesses t ($25\,nm < t < 400\,nm$) and achieved excellent electrical resistivity ($\rho = 0.5$ mΩ cm), optical transmittance ($T > 80\%$), structural quality (FWHM = 0.11°), and a relatively large mobility (24.9 cm^2/Vs). These comprehensive properties are better than those reported for other rare-earth, 5*d* transition metal (e.g., Nb and Ta) and Sb-doped $BaSnO_3$ thin films as of now. Our results demonstrate that Nd-doping is an alternative effective approach to achieve excellent comprehensive properties of $BaSnO_3$-based perovskite-type transparent conductive thin films.

The $Nd_{0.07}Ba_{0.93}SnO_3$ (NBSO) ceramic target was prepared by the conventional solid-state reaction method using Nd_2O_3 (99.9%), $BaCO_3$ (99.8%), and SnO_2 (99.95%) as starting materials. Pulsed laser deposition (PLD) apparatus equipped with a KrF ($\lambda = 248$ nm) excimer laser was employed to grow NBSO thin films on double-side polished 0.5-mm $SrTiO_3$ (STO) (001) single-crystal substrates (Hefei Kejing Materials Technology Co., Ltd., China). During film deposition, the laser energy density (1.5 J/cm^2), the repetition rate (2 Hz), and the substrate-to-target distance (5 cm) were kept constant in order to systematically optimize the substrate temperature, oxygen pressure, and deposition time. After film deposition, NBSO films were *in situ* annealed for 20 min and slowly cooled down to room temperature with the same oxygen pressure.

The crystalline quality and epitaxial properties of NBSO films were characterized through x-ray diffraction (XRD) θ-2θ, ω, and ϕ scans as well as the reciprocal space mapping (RSM) using a PANalytical X'Pert PRO x-ray diffractometer equipped with Cu Kα1 radiation ($\lambda = 1.5406$ Å). The surface morphology and roughness of NBSO films were measured using an atomic force microscope (MFP-3D, Asylum Research). The film thickness and microstructure near the interface region were characterized by cross-sectional transmission electron microscopy (TEM) using a Tecnai G2 F20 S-Twin transmission electron microscope. The distribution of the Ba, Nd, Sn elements was determined using an x-ray energy dispersive spectrometer (EDS) (Oxford Aztec X-Max80). The carrier density, mobility, and resistivity of NBSO films were measured using the physical property measurement system (PPMS-9, Quantum Design). Optical transmittance spectroscopy was measured using a U-4100 UV-vis-NIR spectrophotometer.

Oxygen pressure is one of the most important parameters that strongly influence the carrier density and resistivity of $BaSnO_3$-based thin films. We thus kept the substrate temperature (800 °C) and deposition time (30 min) constant to probe into the effects of oxygen pressure (P_{O2}) on the NBSO films' morphology and conductivity. Figure 1(a) shows a representative photography of a NBSO thin-film sample, which is deposited at $P_{O2} = 10$ Pa. The film is obviously transparent in the visible spectrum. We employed TEM and AFM to measure the thickness and roughness of the 10-Pa film. Figure S1(a) shows that the thickness is approximately 100 nm for 30 min deposition time, resulting in a growth rate of 3.33 nm/min. The AFM image shows that the 10-Pa film has a very smooth surface with a root mean square (RMS) roughness of 0.46 nm [Fig. S1(b), supplementary material]. Figure 1(c) shows XRD θ-2θ scan patterns of the NBSO films deposited at various oxygen pressures. The results indicate that all the NBSO films are single phase and highly *c*-axis oriented. XRD ϕ scans show that the four-fold diffraction peaks of the NBSO film occur at the same azimuthal angle as that of the STO substrates [Fig. 1(d)], indicating epitaxial growth of the NBSO film on the STO substrate. The RSM result [Fig. S1(c), supplementary material] suggests in-plane lattice relaxation due to the relatively large lattice mismatch between the STO and the NBSO. Figure 1(e) shows the rocking curves taken on the NBSO (002) diffraction peaks. The full-width at half-maximum (FWHM) for NBSO films prepared with different oxygen pressures is shown in the inset of Fig. 1(e). With increasing oxygen pressure from 1 to 10 Pa, the FWHM of the (002) diffraction peaks decreases significantly and increases upon a further increase in the oxygen pressure up to 30 Pa. The minimum value of FWHM is only 0.079° for the 10 Pa NBSO films prepared at 10 Pa, which is the smallest value for rare-earth and Nb-, Ta-, and Sb-doped $BaSnO_3$ films (Table I).[19–28] The high-resolution TEM image shows that the interface between the NBSO film and the STO substrate is nearly perfect [Fig.

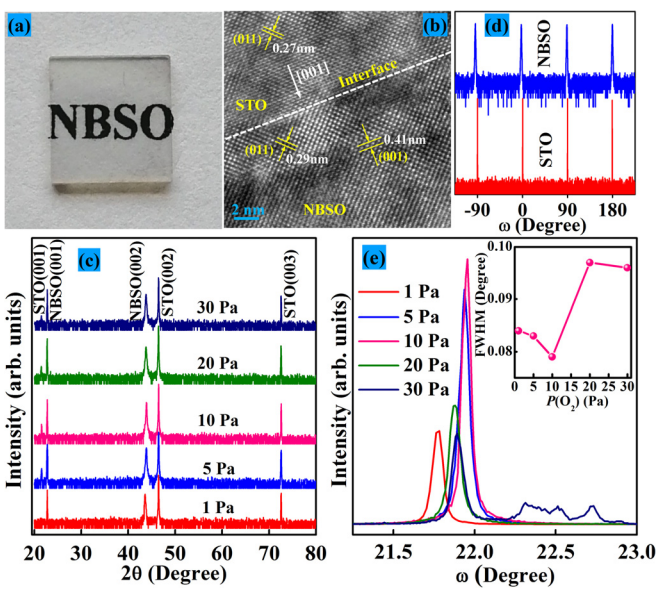

FIG. 1. Structural properties of the NBSO(100 nm)/STO thin-film sample prepared at an oxygen pressure of 10 Pa and a substrate temperature of 800 °C. (a) A photography of the thin-film sample. (b) A TEM image taken near the interface region. (c) XRD θ-2θ scan patterns. (d) XRD ϕ scan patterns. (e) XRD ω-scan rocking curves taken on the NBSO(002) diffraction peak. The inset shows the FWHM values as a function of oxygen pressure.

1(b)]. EDS measurements show that the distribution of Nd ions in the film is homogeneous [Fig. S2, supplementary material]. All these results establish that the NBSO film is high quality.

Electronic transport and optical transmittance were measured to understand the effects of oxygen pressure on the optical transparency and conductivity of NBSO films prepared with different oxygen pressures. Figures 2(a)–2(c) show the temperature dependence of the electrical resistivity (ρ), carrier density (n), and Hall mobility (μ) for NBSO films, respectively. Among these parameters, a simple function $\rho = 1/ne\mu$ (where e is the electron charge) is employed to explain their relationship. The temperature-dependent resistivity curves for all oxygen pressures show more or less metallic behaviors,[29,30] which agrees with the previously reported results for rare-earth and Ta, Nb, and Sb-doped $BaSnO_3$ systems. For the two high-resistivity curves (5 and 30 Pa), resistivity upturn tendencies can be found in the low-temperature region, which indicates metal-insulator transitions. The metallic behaviors can be explained by the formation of a degenerate band due to the introduction of a large concentration of carriers into the system while the insulating behavior at low temperatures may be contributed by the weak localization of electronic states.[29,30] Although the variation of the resistivity with oxygen pressure is complicated at 300 K, the resistivity and carrier density show extremum for $P_{O2} = 10$ Pa. It is noted that the crystalline quality also shows the best for $P_{O2} = 10$ Pa, which implies that the conductivity is related to the crystalline quality of NBSO films. For the aforementioned thin films, the maximum room-temperature carrier concentration of $1.85 \times 10^{20}\,cm^{-3}$ was obtained for the 10-Pa NBSO film, which is suitable for use as transparent thin-film electrodes.[11] The mobility also shows oxygen-pressure-related behaviors, e.g., the maximum room-temperature mobility ($20.6\,cm^2/Vs$ at $T = 300$ K) is achieved for the film deposited at 20 Pa. While for the films deposited at 10-Pa oxygen pressure, the mobility ($15.9\,cm^2/Vs$ at $T = 300$ K) is lower than that for $P_{O2} = 20$ Pa. Note that the mobility is not only dependent on the grain boundary scatterings but also on ionized impurity scatterings. The increase in crystalline quality would reduce the grain boundary scatterings, favoring higher mobility. However, with a further increase in the oxygen pressure, the crystalline quality decreases as reflected by the increase in the FWHM values. Nevertheless, higher oxygen pressure reduces the oxygen vacancies and thus reduces the ionized scatterings. Both of these two scattering mechanisms evolve with oxygen pressure, leading to the highest mobility for the 20-Pa thin-film sample.[31] To summarize, the best deposition oxygen pressure for the NBSO is 10 Pa, based on which $\rho = 1.85$ mΩ cm, $n = 1.85 \times 10^{20}\,cm^{-3}$, and a relatively high mobility of $15.9\,cm^2/Vs$ are achieved at $T = 300$ K.

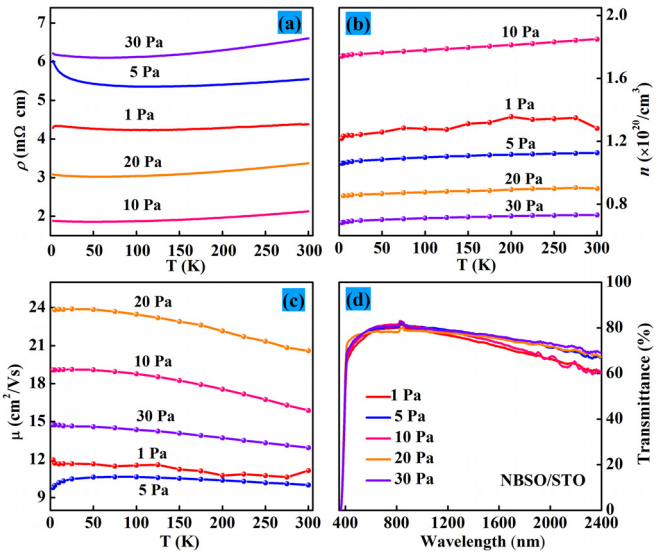

FIG. 2. Temperature dependence of (a) electrical resistivity, (b) carrier density, and (c) Hall mobility for NBSO films deposited with different oxygen pressures. (d) The optical transmittance of NBSO/STO thin-film samples in the wavelength range of 350–2400 nm.

Figure 2(d) shows the optical transmittance of the NBSO films in the wavelength range of 350–2400 nm. The transmittance (T) of the NBSO films T_{NBSO} ($T_{NBSO} = T_{NBSO/STO}/T_{STO}$) is estimated to be more than 80% in the visible wavelength range. In the near-infrared region, the transmittance slightly decreases probably due to the free electron absorption,[27] which means that the increase in the carrier density results in the decrease in the transmittance in the near-infrared region.

Further, we fixed the deposition oxygen pressure at 10 Pa to explore the effects of deposition temperature on the crystallographic and transparent conductive properties of

TABLE I. Volume carrier density, Hall mobility, electrical resistivity, optical transmittance, and full-width at half-maximum (FWHM) of XRD rocking curves taken on the (002) diffraction patterns of $BaSnO_3$-based transparent thin films.

$BaSnO_4$	n ($\times 10^{20}/cm^3$)	μ (cm^2/Vs)	ρ (mΩ cm)	T	FWHM
Sb-0.07 on the $SrTiO_3$ substrate[19]	2.43	1.75	2.43	70%	
Ta-0.07 on the MgO substrate[20]	5	4.92	2.53	70%	0.55°
Nb-0.05 on the MgO substrate[21]	6.59	19.65	0.48	80%	0.43°
La-0.01 on the $BaSnO_3$ substrate[22]	1.3	100	0.5	…	…
La-0.04 on the $SrTiO_3$ substrate[23]	4.4	70	0.3	…	…
Sm-0.04 on the MgO substrate[24]	2.259	3.52	7.8	80%	0.55°
Gd-0.07 on the MgO substrate[25]	0.8909	11.35	6.2	80%	…
La-0.07 on the $SmScO_3$ substrate[26]	1.38	10.11	4.4	…	0.09°
La-0.07 on the $SrTiO_3$ substrate[26]	1.36	5.8	7.8	…	0.09°
La-0.07 on the MgO substrate[27]	8.377	41.06	0.12	75%	0.61°
La-0.07 on the $SrTiO_3$ substrate[28]	2	0.69	4	95%	0.57°
Nd-0.07 on (This work) the $SrTiO_3$ substrate	5.03	24.86	0.5	>80%	0.11°

BSNO films. As discussed in previous paragraphs, the FWHM values of rocking curves [Fig. 3(a)] around NBSO (002) diffraction peaks reflect the crystalline quality of the films. As illustrated in Fig. 3(b), the FWHM values initially decrease and then increase with the increasing deposition temperature from 700 to 850 °C, showing the smallest FWHM value of 0.085° for the film prepared at 800 °C, indicating that the atom occupation is probably maximized at 800 °C. It is noted that the NBSO films deposited at 750 °C shows the smallest RMS roughness of 0.37 nm (Fig. S3, supplementary material).

Moreover, we employed electronic transport and optical measurements to evaluate the transparent conductive properties of the NBSO films deposited at various temperatures. Figure 3(c) shows the electron concentration, resistivity, and mobility at $T = 300$ K as a function of the deposition temperatures. Obviously, the resistivity decreases significantly as the deposition temperature increases from 700 to 825 °C. The lowest room-temperature resistivity (0.5 mΩ cm) is obtained in the 825 °C-deposited films. The carrier concentration increases gradually as the deposition temperature increases from 700 to 825 °C, and the maximum room-temperature carrier concentration of $5.04 \times 10^{20}\,\mathrm{cm}^{-3}$ was achieved for the 825 °C-deposited film. The same deposition-temperature relationship was observed for the carrier mobility, which yields the largest room-temperature value of 24.9 cm^2/Vs at 825 °C. Therefore, via tuning the deposition temperature, we can tune the conductivity of the NBSO films, which is also dependent on the crystalline quality of the NBSO films. Moreover, we measured the optical transmittance in the wavelength range of 350–2400 nm. The transmittance (T) of the NBSO films T_{NBSO} ($T_{\mathrm{NBSO/STO}}/T_{\mathrm{STO}}$) is estimated to be more than 80% in the visible range [Fig. 3(d)], which is close to that of the STO substrate, illustrating the good transparency of the NBSO films.

Next, we kept the deposition temperature at 825 °C and the oxygen pressure at 10 Pa to further grow NBSO films with various deposition times. The deposition time was set as 7.5, 15, 30, 60, and 120 min, respectively. As aforementioned, we still employ the FWHM of rocking curves [Fig. 4(a)] to evaluate the crystalline quality. As illustrated in Fig. 4(b), the FWHM decreases with the increasing deposition time and reaches the minimum at the 60-min deposition time, after which shows a slight upturn. The surface morphology of this film (~200 nm) is shown in Fig. S4 of the supplementary material, where one can find that the RMS roughness is only 1.03 nm. Similarly, we summarized the conductive properties of the NBSO films in Fig. 4(c) to further understand the thickness effects of the BSNO films. As the film thickness increases from 25 to 400 nm, the room-temperature carrier mobility increases from 14.8 to 28.5 cm^2/Vs. The best transport properties are achieved for the 30-min deposited 100-nm film, with the lowest room-temperature ρ of 0.5 mΩ cm and the maximum carrier density of $5.04 \times 10^{20}\,\mathrm{cm}^{-3}$. Figure 4(d) shows the optical transmittance of the NBSO with various thicknesses in the wavelength range of 250–2400 nm. The transmittance (T) of the NBSO films T_{NBSO} ($T_{\mathrm{NBSO/STO}}/T_{\mathrm{STO}}$) is estimated to be more than 80% in the visible range. In the near-infrared range, the transmittance of NBSO films decreases with the increasing film thickness, mainly due to the plasma

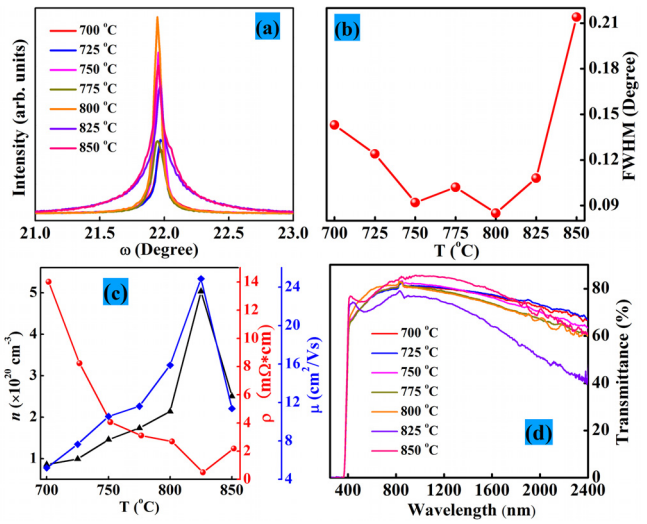

FIG. 3. (a) XRD rocking curves taken on the NBSO (002) diffraction peaks for NBSO films deposited at different substrate temperatures. (b) The FWHM of the XRD rocking curves shown in (a). (c) The electrical resistivity, carrier density, and Hall mobility for NBSO films deposited at different substrate temperatures. (d) The optical transmittance in the wavelength range of 350–2400 nm for NBSO/STO thin-film samples deposited at different substrate temperatures.

resonance effect, which is proportional to the square root of the carrier concentration.[27] The excellent visible light transparency and low room temperature resistivity of the present NBSO films would be one of the alternative materials for next generation transparent conductive applications in optoelectronic industry.

After aforementioned steps of optimizing, we obtained the best transparent conductive NBSO films deposited on STO substrates with a deposition time of 30 min (approximately 100 nm), an oxygen pressure of 10 Pa, and a substrate temperature of 825 °C. Specifically, the NBSO films possess a low room-temperature resistivity of 0.5 mΩ cm, a high

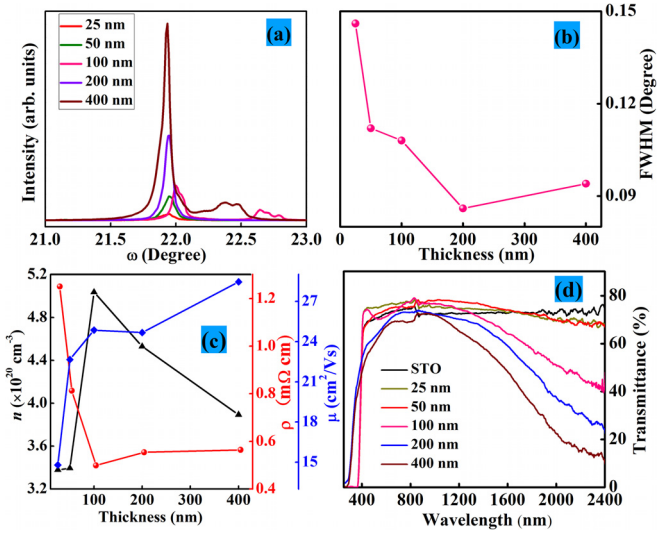

FIG. 4. (a) XRD rocking curves taken on the NBSO (002) diffraction peaks for NBSO films with different thicknesses. (b) The FWHM of the XRD rocking curves shown in (a). (c) The electrical resistivity, carrier density, and Hall mobility for NBSO films with different thicknesses. (d) The optical transmittance in the wavelength range of 350–2400 nm for NBSO/STO thin-film samples with different film thicknesses and a bare double-polished STO substrate.

carrier concentration of $5.04 \times 10^{20}\,\mathrm{cm}^{-3}$, a relatively high mobility of $24.9\,\mathrm{cm}^2/\mathrm{Vs}$, and a high optical transmittance of >80%. A comparison of the structural, optical, and electrical properties of the present 100-nm NBSO film with other rare-earth and Ta, Nb, and Sb-doped $BaSnO_3$ films is shown in Table I, from which one can find that the comprehensive properties of the NBSO film are excellent.

In conclusion, the oxygen pressure, substrate temperature, and film thickness have been systematically optimized to achieve excellent structural, optical, and electrical properties of $Ba_{0.93}Nd_{0.07}SnO_3$ (NBSO) thin films. We found that the NBSO films prepared at an oxygen pressure of 10 Pa and a substrate temperature of 825 °C show the best crystallization (FWHM = 0.11), lowest resistivity (0.5 mΩ cm), relatively large mobility ($24.9\,\mathrm{cm}^2/\mathrm{Vs}$), and excellent optical transmittance ($T > 80\%$) in the visible wavelength region. These comprehensive properties are superior to those of other rare-earth and Ta, Nb, and Sb-doped $BaSnO_3$ thin films as of now. Our results demonstrate that Nd-doped $BaSnO_3$ is one of the excellent perovskite-type transparent conductive materials, which may have potential applications in optoelectronic devices.

See supplementary material for TEM and AFM images, reciprocal space mapping (RSM), EDS elemental mapping of Nd, Ba, and Sn for the 100-nm NBSO films prepared at 10 Pa and 800 °C substrate temperature, AFM images of the NBSO thin-film sample prepared at 10 Pa oxygen pressure and 750 °C substrate temperature, and the AFM image of the 200-nm NBSO thin-film sample prepared at an oxygen pressure of 10 Pa and a substrate temperature of 825 °C.

This work was supported by the National Natural Science Foundation of China (Grant Nos. 51572278, 11574214, and 51872278). The support from Jiangxi Key Laboratory for Two-Dimensional Materials and Devices and Jiangxi Engineering Laboratory for Advanced Functional Thin Films is also acknowledged.

[1]D. S. Ginley and C. Bright, MRS Bull. **25**, 15 (2000).
[2]T. Minami, MRS Bull. **25**, 38 (2000).
[3]K. Nomura, H. Ohta, K. Ueda, T. Kamiya, M. Hirano, and H. Hosono, Science **300**, 1269 (2003).
[4]I. Hamberg and C. G. Granqvist, J. Appl. Phys. **60**, R123 (1986).
[5]R. F. Service, Science **310**, 1762 (2005).
[6]A. J. Freeman, K. R. Poeppelmeier, T. O. Mason, R. P. H. Chang, and T. J. Marks, MRS Bull. **25**, 45 (2000).
[7]K. Ellmer, Nat. Photonics **6**, 809 (2012).
[8]H. Mizoguchi, T. Kamiya, S. Matsuishi, and H. Hosono, Nat. Commun. **2**, 470 (2011).
[9]A. Suzuki, T. Matsushita, T. Aoki, A. Mori, and M. Okuda, Thin Solid Films **411**, 23 (2002).
[10]U. Betz, M. K. Olsson, J. Marthy, M. F. Escola, and F. Atamny, Surf. Coat. Technol. **200**, 5751 (2006).
[11]T. Minami, Semicond. Sci. Technol. **20**, S35 (2005).
[12]W. Ramadan, S. B. Ogale, S. Dhar, S. X. Zhang, D. C. Kundaliya, I. Satoh, and T. Venkatesan, Appl. Phys. Lett. **88**, 142903 (2006).
[13]B. N. Mbenkum, N. Ashkenov, M. Schubert, M. Lorenz, H. Hochmuth, D. Michel, M. Grundmann, and G. Wagner, Appl. Phys. Lett. **86**, 091904 (2005).
[14]H. Tetsuka, Y. J. Shen, K. Tezuka, H. Imoto, and K. Wasa, J. Vac. Sci. Technol. A **24**, L4 (2006).
[15]J. Ravichandran, W. Siemons, H. Heijmerikx, M. Huijben, A. Majumdar, and R. Ramesh, Chem. Mater. **22**, 3983 (2010).
[16]E. Baba, D. Kan, Y. Yamada, M. Haruta, H. Kurata1, Y. Kanemitsu, and Y. Shimakawa, J. Phys. D: Appl. Phys. **48**, 455106 (2015).
[17]L. Zhang, Y. J. Zhou, L. Guo, W. W. Zhao, A. Barnes, H. T. Zhang, C. Eaton, Y. X. Zheng, M. Brahlek, H. F. Haneef, N. J. Podraza, M. H. W. Chan, V. Gopalan, K. M. Rabe, and R. Engel-Herbert, Nat. Mater. **15**, 204 (2016).
[18]H. R. Liu, J. H. Yang, H. J. Xiang, X. G. Gong, and S. H. Wei, Appl. Phys. Lett. **102**, 112109 (2013).
[19]Q. Z. Liu, J. M. Dai, Z. L. Liu, X. B. Zhang, G. P. Zhu, and G. H. Ding, J. Phys. D: Appl. Phys. **43**, 455401 (2010).
[20]Q. Z. Liu, F. Jin, G. Y. Gao, B. Li, Y. X. Zhang, and Q. C. Liu, J. Alloys Compd. **684**, 125 (2016).
[21]B. Li, Q. Z. Liu, Y. X. Zhang, Z. L. Liu, and L. Geng, J. Alloys Compd. **680**, 343 (2016).
[22]W. J. Lee, H. J. Kim, E. Sohn, T. H. Kim, J. Y. Park, W. Park, H. Jeong, T. Lee, J. H. Kim, K. Y. Choi, and K. H. Kim, Appl. Phys. Lett. **108**, 082105 (2016).
[23]H. J. Kim, U. Kim, H. M. Kim, T. H. Kim, H. S. Mun, B. G. Jeon, K. T. Hong, W. J. Lee, C. J. Ju, K. H. Kimy, and K. Char1z, Appl. Phys. Express **5**, 061102 (2012).
[24]B. Li, Y. X. Zhang, Z. L. Liu, and L. Geng, J. Alloys Compd. **708**, 1117 (2017).
[25]Q. Z. Liu, J. M. Dai, H. Li, B. Li, Y. X. Zhang, K. Dai, and S. Chen, J. Alloys Compd. **647**, 959 (2015).
[26]P. V. Wadekar, J. Alaria, M. O'Sullivan, N. L. O. Flack, T. D. Manning, L. J. Phillips, K. Durose, O. Lozano, S. Lucas, J. B. Claridge, and M. J. Rosseinsky, Appl. Phys. Lett. **105**, 052104 (2014).
[27]Q. Z. Liu, F. Jin, J. M. Dai, B. Li, L. Geng, and J. J. Liu, Superlattices Microstruct. **96**, 205 (2016).
[28]H. F. Wang, Q. Z. Liu, F. Chen, G. Y. Gao, W. B. Wu, and X. H. Chen, J. Appl. Phys. **101**, 106105 (2007).
[29]P. A. Lee and T. Ramakrishnan, Rev. Mod. Phys. **57**, 287 (1985).
[30]N. F. Mott, Rev. Mod. Phys. **40**, 677 (1968).
[31]D. H. Zhang and H. L. Ma, Appl. Phys. A **62**, 487 (1996).